Comparison of Heat Source Model for Numerical Modeling of Selective Laser Melting of IN625 Superalloy

LI Binxun[1,2*], *SUN Yujing*[1,2], *DU Jin*[1,2], *XIA Yan*[1,2], *SU Guosheng*[1,2], *ZHANG Qing*[3]

1. School of Mechanical Engineering, Qilu University of Technology (Shandong Academy of Sciences), Jinan 250353, P.R. China;
2. Shandong Institute of Mechanical Design and Research, Jinan 250031, P.R. China;
3. Engineering Training Center, Shandong University, Jinan 250002, P.R. China

(Received 18 December 2023; revised 20 March 2024; accepted 10 April 2024)

Abstract: The selection of heat source model is very important to accurately predict the distribution of temperature field and melting pool geometry in the numerical modeling of additive manufacturing process. The surface model, volumetric model and double-ellipsoid model are selected for comparison and analysis. These three heat source models are progarmmed as user-defined subroutines with Abaqus/Standard simulation software to predict the peak temperature and melting pool geometry during selective laser melting (SLM) of IN625. The comparison between simulation and experimental results shows that double-ellipsoid model can predict the melting pool geometry well, while the volumetric model provides comparative peak temperature predictions. In contrast, the surface model exhibits significant deviations in both melting pool geometry and peak temperature. The findings in this research highlight the need for model calibration or modification to enhance efficiency and accuracy before further research can be conducted.

Key words: heat source model; numerical modeling; IN625; temperature; melting pool geometry

CLC number: TG456.7 **Document code:** A **Article ID:** 1005-1120(2024)02-0174-10

0 Introduction

Metal additive manufacturing (AM), as one of the emerging advanced manufacturing technologies, has demonstrated the great capability of manufacturing components with intricate geometry and free-form surfaces in comparison to conventional manufacturing processes, which has found successful application in various industries such as aerospace, automotive and medical devices[1-3]. However, despite its benefits, additively manufactured components face significant challenges in terms of quality and mechanical properties, primarily due to internal defects, distortion, and high thermal residual stress[4].

In terms of additive manufacturing, selective laser melting (SLM) is one of the commonly utilized techniques for metal additive manufacturing including widely used nickel-based superalloys in the aerospace industry, which involves high-density energy, melting, liquidus material flowing, vaporization, and solidification[5]. Therefore, it is unrealistic to observe the complicated interaction experimentally between laser and metal powders. Under this condition, the finite element modeling is proposed as an efficient method to fulfill the purpose, and as far as AM modeling is concerned, various numerical modeling methods have been developed and used by many researchers. These methods can be generally classified as mesh-based numerical method[6-9] and mesh-free modeling strategy[10-12], to be capable of feedbacking high fidelity solutions. Since the laser heat source typically features with local concentration, transient and fast-moving, it develops the ten-

*Corresponding author, E-mail address: libx@qlu.edu.cn.

How to cite this article: LI Binxun, SUN Yujing, DU Jin, et al. Comparison of heat source model for numerical modeling of selective laser melting of IN625 superalloy[J]. Transactions of Nanjing University of Aeronautics and Astronautics, 2024, 41(2): 174-183.

http://dx.doi.org/10.16356/j.1005-1120.2024.02.004

dency to generate a large gradient of non-uniform temperature distribution as well as the thermal-induced stress. However, despite the numerical modeling methods, there is no doubt that the proper heat source model selection plays an important role in reliably describing the thermodynamic behavior of the melting pool.

So far, several heat source models have been developed by many scholars to define heat transfer in the melting pool and powder bed, including Gaussian surface heat source, double-ellipsoidal heat source, and many other geometrically modified volumetric heat sources[13-15]. Considering the quite limited layer thickness of the powder, the surface heat source model has been widely adopted to simulate the SLM process[16-19]. Chaurasia et al.[20] used a 2-D surface heat source model with a Gaussian shape to model laser surface melting of IN625 with and without considering fluid dynamics and obtain comparatively reasonable results. In addition, Fu and Guo[21] simulated the melting pool dimensions in terms of pool width, length, and depth in SLM of Ti-6Al-4V using surface heat flux with the highlighted extremely higher surface temperature. In practice, the laser heat flux will penetrate through the shallow powder thickness due to heat conductivity and particle surface reflection and therefore results in the remelting of the previous solidification layer[22]. Based on the surface heat model, the volumetric heat surface model with Gaussian distribution was developed[23-24]. When modeling laser butt welding of stainless steel, the presented volumetric model in this study predicted the peak temperature and residual stress profile against the measured values[25]. In addition, another volumetric heat source model commonly employed by researchers is the double-ellipsoid type[26-29]. Dunbar et al.[30] utilized a double-ellipsoid model combining mechanical analysis to simulate the built part distortion and the model results matched well with the experimental measurements. Moreover, the double-ellipsoid heat model proposed first by Goldak et al.[31] has also been validated against many experimental investigations in metal AM[32-33]. It can be seen that, although various heat source models have been adopted by many scholars in the numerical modeling of AM processes, even for the same metal materials and AM technique, the efficiency and accuracy of different types of heat flux models deserve further investigation and comparison.

In this study, a three-dimensional finite element model for the fulfillment of SLM IN625 is built in Abaqus/Standard. The surface heat source model, volumetric model, and double-ellipsoid model are respectively presented and programmed as a user-defined subroutine implemented into Abaqus for modeling heat transfer in the IN625 powder bed. The predicted melting pool geometry and peak temperature are extracted validating against the experimental results cited from open literatures.

1 Heat Source Model for SLM

To model the laser heat distribution and transfer on the powder bed, the three most commonly used heat source models including the surface heat source model, volumetric heat source model, and double-ellipsoid heat source model have been selected for comparison in terms of efficiency and accuracy.

The frequently utilized surface heat flux equation with Gaussian distribution is listed as

$$q(x,y)=\frac{2AP}{\pi\omega^2}\exp\left(-\frac{2\left((x-x_0)^2+(y-y_0)^2\right)}{\omega^2}\right) \tag{1}$$

where q is the laser intensity, A the coefficient of laser absorption, P the nominal laser power, ω the laser spot radius, and (x_0, y_0) the coordinate of the laser spot center.

Based on the surface heat source model, the volumetric heat source model with Gaussian form takes into account the penetration of the laser beam into the powder bed, as shown in Fig.1(a), which is defined as

$$q(x,y,z)=\frac{2AP}{\pi\omega^2\eta}\exp\left(-2\frac{(x-x_0)^2+(y-y_0)^2}{\omega^2}\right)\cdot\exp\left(-\frac{|z|}{\eta}\right) \tag{2}$$

where η is the depth of laser beam penetration.

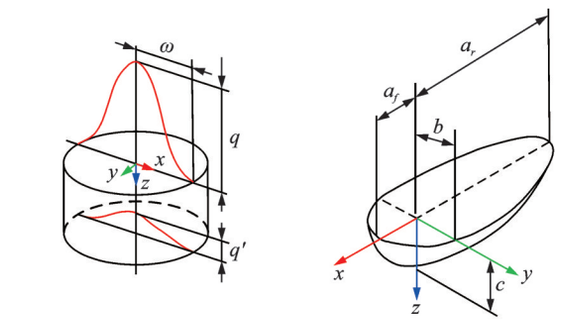

(a) Volumetric shape with Gaussian (b) Double-ellipsoid shape

Fig.1 Schematic of heat source models

The double-ellipsoid heat source model was presented by Goldak et al.[31] to accurately capture the melting pool geometry, as shown in Fig.1(b), and the equation of this model includes two parts, named the front part and rear part, respectively.

The front part of the double-ellipsoid can be written as

$$q(x,y,z)=\frac{6\sqrt{3}\,f_{\mathrm{f}}AP}{a_{\mathrm{f}}bc\pi\sqrt{\pi}}\exp\left(-\frac{3(x-x_0)^2}{a_{\mathrm{f}}^2}+\frac{3(y-y_0)^2}{b^2}+\frac{3(z-z_0)^2}{c^2}\right)\quad x\geqslant 0 \tag{3}$$

While the rear part can be expressed as

$$q(x,y,z)=\frac{6\sqrt{3}\,f_{\mathrm{r}}AP}{a_{\mathrm{r}}bc\pi\sqrt{\pi}}\exp\left(-\frac{3(x-x_0)^2}{a_{\mathrm{r}}^2}+\frac{3(y-y_0)^2}{b^2}+\frac{3(z-z_0)^2}{c^2}\right)\quad x<0 \tag{4}$$

where a_{f} and a_{r} denote the semi-axes of the front and rear ellipsoidal, respectively; f_{f} and f_{r} the ratios of controlling heat flux flows into the front and rear parts of the heat source, respectively; b and c the lengths of semi-axes along the y and z directions, respectively. The model constants associated with the above-mentioned equations are cited and listed in Table 1.

Table 1 Constants for three heat source models

Heat source model	Variable	Value	Source
Surface model	A	0.3	Ref.[21]
Volumetric model	A	0.3	Ref.[21]
	η	0.4	Ref.[34]
Double-ellipsoid model	a_{f}/μm	276	Refs.[35-36]
	a_{r}/μm	1 520	
	b/μm	160	
	c/μm	160	
	f_{f}	1.4	
	f_{r}	0.6	

2 Finite Element Modeling

In this research, the surface type, volumetric type, and double-ellipsoid type are selected to compare their efficiency and accuracy during the modeling of the SLM of IN625 nickel-based alloy. As shown in Fig.2, a 3D FE model with a geometrical size of 10 mm × 2 mm × 1 mm is created using Abaqus/Standard. Taking into account both the computation time and grid independence, the region located in the laser impact domain is meshed with 100 μm in length and 25 μm in width and a bias along the depth direction, with a total number of 193 456 elements. The element type of DC3D8 is assigned to the FE model. The "birth and death element control" function built-in Abaqus is activated to simulate the conversion from powder to solid. The above-mentioned three heat source models are respectively programmed as user-defined subroutine DFLUX and subsequently integrated into Abaqus. To simplify the modeling procedures, the assumptions of the numerical model include (i) The liquid in the melting pool is considered as viscous incompressible Newtonian fluid, (ii) composition changes and elements loss due to evaporation and spattering during melting are ignored, (iii) the coefficient of surface tension in the melting pool has not been considered in the model. The required thermo-mechanical properties of IN625 are listed in Table 2.

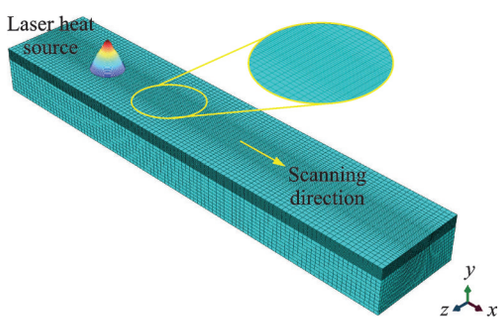

Fig.2 3D FE model in SLM of IN625

Table 2 Thermo-mechanical properties of IN625 powder

Material property	Value
Density ρ/(kg•m^{-3})	8 440
Liquidus temperature T_L/℃	1 450
Solidus temperature T_S/℃	1 290
Specific heat C_p/(J•kg^{-1}•℃$^{-1}$)	338.98 + 0.243 7T ($T \leqslant T_S$) 735 ($T \geqslant T_L$)
Thermal conductivity k/(W•m^{-1}•℃$^{-1}$)	5.331 + 0.001 5 T ($T \leqslant T_S$) 30.05 ($T \geqslant T_L$)
Latent heat of fusion/(J•kg^{-1})	227 × 10^3
Thermal expansion coefficient β_T/℃$^{-1}$	1.28 × 10^{-5}

The SLM processing parameters include the scanning speed of 100 mm/s and laser powder of 300, 400, and 500 W, respectively, which correspond to those used in Ref.[20]. The laser spot diameter is 500 μm. The simulated molten pool geometry and temperature using various heat source models are extracted to compare with the experimental data for accuracy validation.

3 Results and Discussion

During metal AM, the melting pool in which the solid particles change to liquid provides substantial information for a profound understanding of the AM process[37-38]. In general, the melting pool geometry (width and depth) and peak temperature are the typical indexes used for model validation. A typical simulated temperature contour of SLMed IN625 is shown in Fig.3, indicating the melting pool shape and geometrical characteristics.

Fig.4 shows the top view (x-y plane) of the transient temperature distribution using various heat source models. As the laser heat source moves from left to right, a "comet tail" profile can be noticed. In addition, the steep temperature gradient is highly prominent ahead of the laser beam, and the good thermal conductivity as well as the Marangoni's flow induced by strong surface tension results in the expanded melting pool size[39-40].

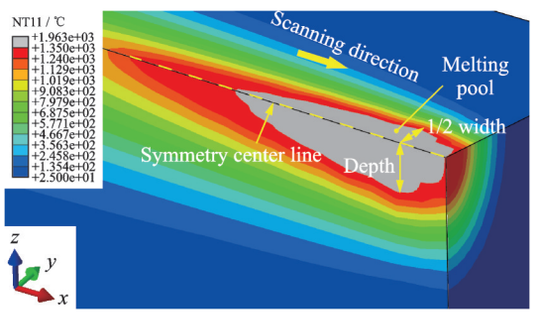

Fig.3 Characterization of melting pool geometry

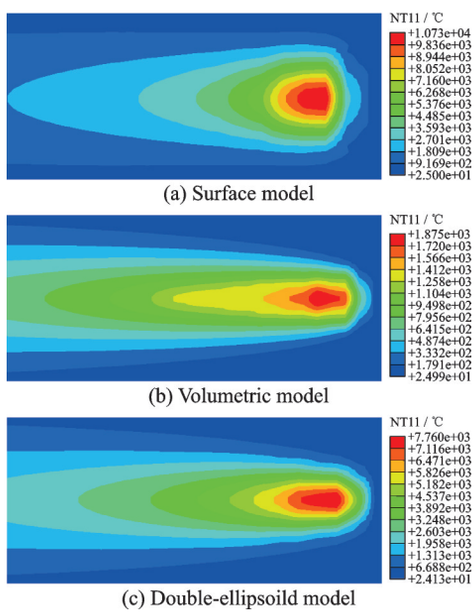

Fig.4 Top view of molten pool geometry with different heat source models (P=500 W)

Fig.5 shows the simulated temperature distribution contour of the cross-section using different heat source models under various SLM processing parameters. The white dot lines within the contour image are the liquidus line corresponding to the liquidus temperature 1 350 ℃ of IN625 powder. According to the legend, the predicted highest surface temperature is corresponding to the surface model regardless of SLM processing parameters. The findings are expected to be the same as the reports in Ref.[20]. The temperature induced by laser heat flux increases with the increasing of laser power. Since the surface model neglects the heat flux distribution beneath the top surface, all the heat energy focuses on the surface eventually, resulting in the observed extremely high temperature and quite shallow melting pool shape. In contrast, the volumetric and double-ellipsoid models consider the heat pene-

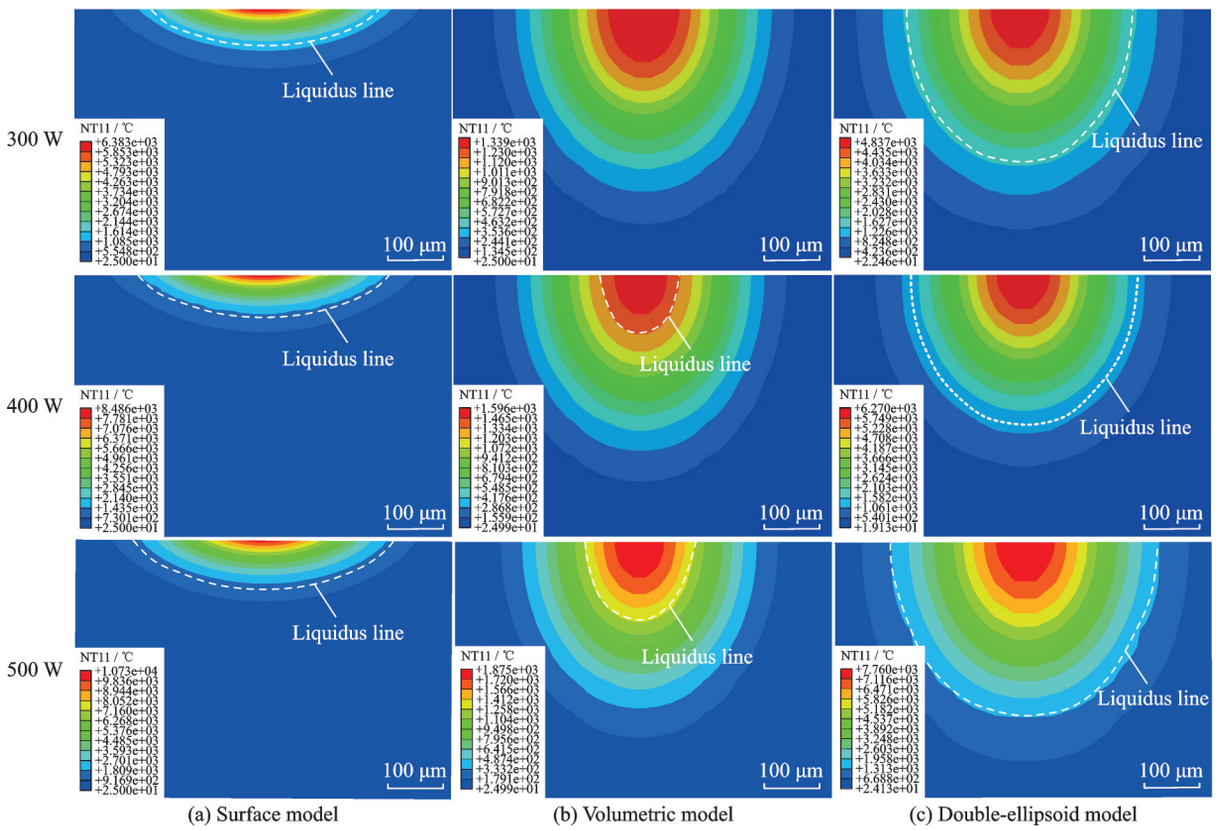

Fig.5 Cross-section view of molten pool geometry with different heat source models at different laser powers

tration in depth due to particle surface reflection, the transient temperature distribution along the Z-direction is much deeper, and thus the expected melting pool depth increases. It should be highlighted that the highest temperature of 1 339 ℃ using volumetric model under laser power 300 W is lower than the liquidus temperature of 1 350 ℃, which suggests the inadequate melting of the powder particles in SLM processes and is supposed to form a mushy zone.

As far as the melting pool geometry and peak temperature are concerned, some detailed information is listed in Table 3. Based on the data in Table 3, the predicted melting pool width and depth associated with the double-ellipsoid model show a relatively good agreement with the experimental results in Ref.[20], while a large discrepancy appears with surface and volumetric models. Specifically, the predicted melting pool widths using the volumetric model are 324, 372 and 500 μm corresponding to laser power 300, 400 and 500 W, respectively. And the experimental data is 307, 385 and 455 μm with an absolute error of 5.5%, 3.4% and 9.89%, respectively. For the melting pool depth, the predicted values are 225, 246 and 287 μm and correspondingly the experimental data are 179, 274 and 321 μm with an absolute error of 25.7%, 10.2% and 10.59%, which proves the accuracy of the double-ellipsoid model in predicting the melting pool dimensions. After all, Eqs.(2—4) themselves describing the volumetric models consider the heat penetration depth. In terms of the peak temperature, it is the volumetric model that is in agreement with experimental data in Ref.[20], while the simulated temperatures with double-ellipsoid and surface models show great deviation. To be more specific, the absolute errors between simulation with volumetric model and experiment under different laser powers are 30.1%, 26.5%, and 21.48%, respectively. Although the estimated absolute errors are all greater than the commonly accepted value of 15%, the volumetric model is still proved to be superior to the other two models. It can be derived that, none of the single heat source models presented in this

Table 3 Geometrical dimensions of the melting pool and peak temperature with different heat source models at different laser powers

Heat source model	Width /μm			Depth /μm			Peak temperature/℃		
	300 W	400 W	500 W	300 W	400 W	500 W	300 W	400 W	500 W
Surface model	482	500	550	72	82	100	6 383	8 486	10 730
Volumetric model	—	176	230	12	87	166	1 339	1 596	1 875
Double-ellipsoid model	324	372	500	225	246	287	4 837	6 270	7 760
Ref.[20]	307	385	455	179	274	321	1 916	2 172	2 388

study can satisfy the melting pool geometry and peak temperature predictions against experiments simultaneously. In contrast, the Gaussian heat source model feedbacks the worst predictions. In Ref.[23], the correlation between melt pool geometry or the peak temperature with the energy deposition has been proved. Similarly, Chukkan et al.[25] conducted a combination of 3D conical and cylindrical shell heat source models and produced more accurate results, which confirmed the essentiality of authentic heat source shape description.

Fig.6 plots the temperature distribution profile starting from the top surface deep into the powder bed. The heat source model has a great impact on the temperature gradient. The observed dramatic temperature gradient is found to be related to the surface model, while the insignificant temperature gradient change corresponds to the volumetric model. With the laser power increasing, the melting pool depth increases simultaneously. Meanwhile, it should be pointed out that every single powder layer thickness is merely limited to several ten microns. As a consequence, the input laser flux will cause the remelting of the previously solidified layer. As the melting pool depth continues to increase, more solidified material will be remelted. Material remelting has been proven to have a significant impact on microstructure evolution and residual stress[41-42].

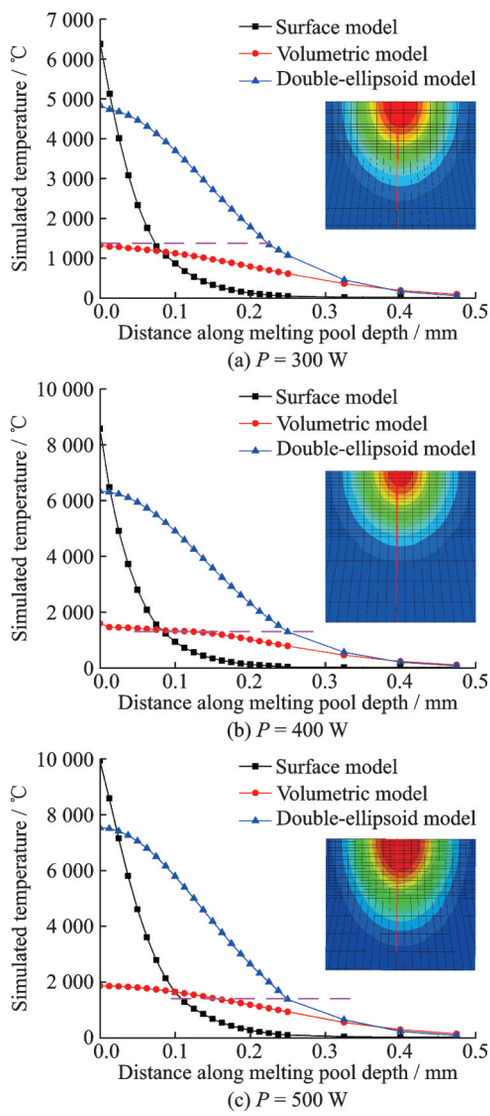

Fig.6 Simulated temperature distribution along Z-direction at different laser powers

Fig.7 plots the temperature variation trend along the Y-direction crossing the melting pool center. Determined by the shape of the laser heat source, it is not hard to imagine that the temperature distribution is symmetrical. The difference in temperature distribution across the melting pool along the Y-direction with various heat source models can be vividly exhibited and a rough comparison of melting pool width can be obtained. In addition, the maximum temperature increases with the rise of laser power from 300 W to 500 W.

Fig.8 provides the simulated melting pool transverse-section profile comparison against the experimentally obtained image. It directly reveals that the melting pool shape using the double-ellipsoid model is comparable regarding the pool width and depth.

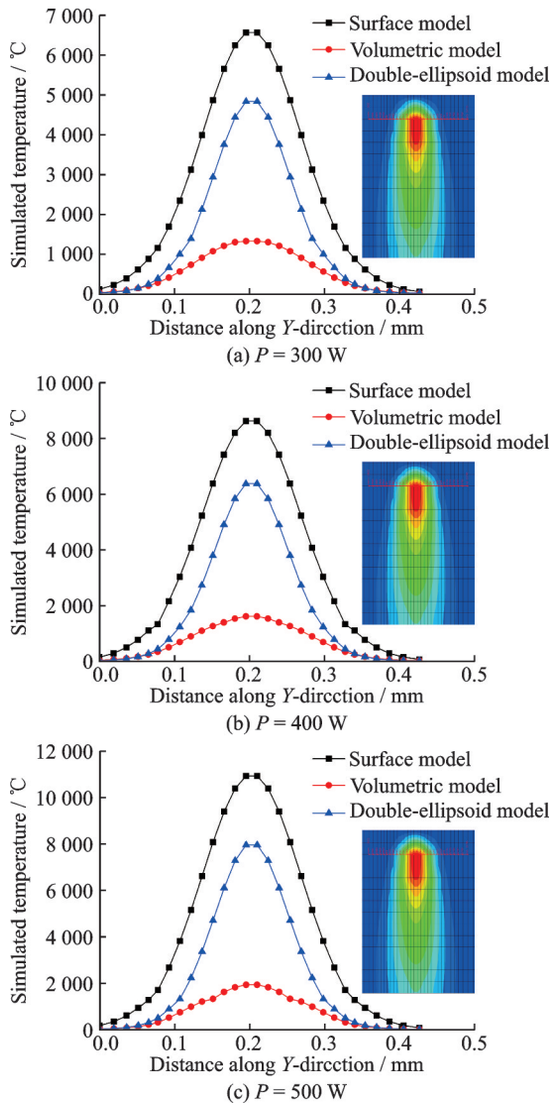

Fig.7 Simulated temperature distribution across the molten pool at different laser powers

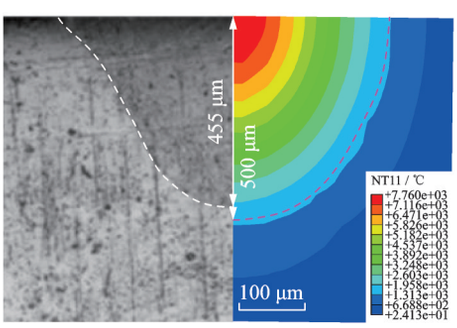

Fig.8 Comparison of the transverse section of the melting pool at laser power of 500 W

4 Conclusions

Three commonly employed heat source models including surface, volumetric, and double-ellipsoid models are selected for accuracy and efficiency comparison in the SLM of IN625 nickel-based superalloys. A 3D FE model with implemented user-defined subroutines DFLUX is created in Abaqus/Standard for numerical modeling and analysis. The main conclusions are as follows:

(1) Concerning the melting pool geometry, the double-ellipsoid model provides acceptable results in comparison to the experimental result cited in the literature, while both the surface and volumetric models show large discrepancies.

(2) The simulated peak temperature with the volumetric model is relatively close to the reported value in the literature in comparison to surface and double-ellipsoid models, even though the absolute errors are all beyond 20% under various SLM processing parameters.

(3) Melting pool dimensions and peak temperature cannot be accurately captured simultaneously with either a double-ellipsoid or volumetric model. To guarantee the numerical model results during the SLM of IN625, the heat source model selection, calibration or modification is a basic prerequisite.

References

[1] ARMSTRONG M, MEHRABI H, NAVEED N. An overview of modern metal additive manufacturing technology[J]. Journal of Manufacturing Processes, 2022, 84: 1001-1029.

[2] GUO Lijie, XU Weichun, QI Chaoqi, et al. Research progress of monitoring and control technology for metal additive manufacturing[J]. Journal of Nanjing University of Aeronautics & Astronautics, 2022, 54(3): 365-377. (in Chinese)

[3] LI J, DUAN C, ZHAO M, et al. A review of metal additive manufacturing application and numerical simulation[J]. IOP Conference Series: Earth and Environmental Science, 2019, 252(2): 022036.

[4] SANAEI N, FATEMI A. Defects in additive manufactured metals and their effect on fatigue performance: A state-of-the-art review[J]. Progress in Materials Science, 2021, 117: 100724.

[5] BAYAT M, THANKI A, MOHANTY S, et al. Keyhole-induced porosities in laser-based powder bed fusion (L-PBF) of Ti6Al4V: High-fidelity modelling and experimental validation[J]. Additive Manufacturing, 2019, 30: 100835.

[6] LEE Y S, LEE K H, CHUNG M G, et al. Extreme gradient boosting-based multiscale heat source modeling for analysis of solid-state phase transformation in additive manufacturing of Ti-6Al-4V[J]. Journal of Manufacturing Processes, 2024, 113: 319-345.

[7] BAIGES J, CHIUMENTI M, MOREIRA C A, et al. An adaptive finite element strategy for the numerical simulation of additive manufacturing processes[J]. Additive Manufacturing, 2021, 37: 101650.

[8] DING D, ZHANG S, LU Q, et al. The well-distributed volumetric heat source model for numerical simulation of wire arc additive manufacturing process[J]. Materials Today Communications, 2021, 27: 102430.

[9] XIE R, CHEN G, ZHAO Y, et al. In-situ observation and numerical simulation on the transient strain and distortion prediction during additive manufacturing[J]. Journal of Manufacturing Processes, 2019, 38: 494-501.

[10] ALMANGOUR B, GRZESIAK D, CHENG J, et al. Thermal behavior of the molten pool, microstructural evolution, and tribological performance during selective laser melting of TiC/316L stainless steel nanocomposites: Experimental and simulation methods[J]. Journal of Materials Processing Technology, 2018, 257: 288-301.

[11] RUSSELL M A, SOUTO-IGLESIAS A, ZOHDI T. Numerical simulation of laser fusion additive manufacturing processes using the SPH method[J]. Computer Methods in Applied Mechanics and Engineering, 2018, 341: 163-187.

[12] ALMANGOUR B, CHENG J, GRZESIAK D, et al. Fundamental study on the development of pure magnesium parts by additive manufacturing: An experimental and computational analysis[J]. Metals and Materials International, 2023, 29(2): 429-443.

[13] WU C, WANG H G, ZHANG Y M. A new heat source model for keyhole plasma arc welding in FEM analysis of the temperature profile[J]. Welding Research, 2006, 85(12): 284-291.

[14] LADANI L, ROMANO J, BRINDLEY W, et al. Effective liquid conductivity for improved simulation of thermal transport in laser beam melting powder bed technology[J]. Additive Manufacturing, 2017, 14: 13-23.

[15] LIU S, ZHU H, PENG G, et al. Microstructure prediction of selective laser melting AlSi10Mg using finite element analysis[J]. Materials & Design, 2018, 142: 319-328.

[16] LI Y, GU D. Parametric analysis of thermal behavior during selective laser melting additive manufacturing of aluminum alloy powder[J]. Materials & Design, 2014, 63: 856-867.

[17] PEYRE P, DAL M, POUZET S, et al. Simplified numerical model for the laser metal deposition additive manufacturing process[J]. Journal of Laser Applications, 2017, 29(2): 022304.

[18] KUNDAKCIOĞLU E, LAZOGLU I, POYRAZ Ö, et al. Thermal and molten pool model in selective laser melting process of Inconel 625[J]. The International Journal of Advanced Manufacturing Technology, 2018, 95: 3977-3984.

[19] SHAHABAD S I, ZHANG Z, KESHAVARZKERMANI A, et al. Heat source model calibration for thermal analysis of laser powder-bed fusion[J]. The International Journal of Advanced Manufacturing Technology, 2020, 106: 3367-3379.

[20] CHAURASIA J K, JINOOP A N, PARTHASARATHY P, et al. Study of melt pool geometry and solidification microstructure during laser surface melting of Inconel 625 alloy[J]. Optik, 2021, 246: 167766.

[21] FU C H, GUO Y B. Three-dimensional temperature gradient mechanism in selective laser melting of Ti-6Al-4V[J]. Journal of Manufacturing Science and Engineering, 2014, 136(6): 061004.

[22] GUSAROV A V, YADROITSEV I, BERTRAND P, et al. Model of radiation and heat transfer in laser-powder interaction zone at selective laser melting[J]. Journal of Heat Transfer, 2009, 131(7): 70-79.

[23] ZHANG Z, HUANG Y, KASINATHAN A R, et al. 3-dimensional heat transfer modeling for laser powder-bed fusion additive manufacturing with volumetric heat sources based on varied thermal conductivity and absorptivity[J]. Optics & Laser Technology, 2019, 109: 297-312.

[24] MOLLAMAHMUTOGLU M, YILMAZ O. Volumetric heat source model for laser-based powder bed fusion process in additive manufacturing[J]. Thermal Science and Engineering Progress, 2021, 25: 101021.

[25] CHUKKAN J R, VASUDEVAN M, MUTHUKUMARAN S, et al. Simulation of laser butt welding of AISI 316L stainless steel sheet using various heat sources and experimental validation[J]. Journal of Materials Processing Technology, 2015, 219: 48-59.

[26] LIU P, CUI X, DENG J, et al. Investigation of thermal responses during metallic additive manufacturing

using a "Tri-Prism" finite element method[J]. International Journal of Thermal Sciences, 2019, 136: 217-229.

[27] GIAROLLO D F, MAZZAFERRO C C, MAZZAFERRO J A. Comparison between two heat source models for wire-arc additive manufacturing using GMAW process[J]. Journal of the Brazilian Society of Mechanical Sciences and Engineering, 2022, 44: 7.

[28] JING H, GE P, ZHANG Z, et al. Numerical studies of the effects of the substrate structure on the residual stress in laser directed energy additive manufacturing of thin-walled products[J]. Metals, 2022, 12(3): 462.

[29] ZHANG Z, GE P, LI J Y, et al. Laser-particle interaction-based analysis of powder particle effects on temperatures and distortions in directed energy deposition additive manufacturing[J]. Journal of Thermal Stresses, 2021, 44(9): 1068-1095.

[30] DUNBAR A J, DENLINGER E R, GOUGE M F, et al. Experimental validation of finite element modeling for laser powder bed fusion deformation[J]. Additive Manufacturing, 2016, 12: 108-120.

[31] GOLDAK J, CHAKRAVARTI A, BIBBY M. A new finite element model for welding heat sources[J]. Metallurgical Transactions B, 1984, 15: 299-305.

[32] ZHAO H, LIU Z, YU C, et al. Finite element analysis for residual stress of TC4/Inconel 718 functionally gradient materials produced by laser additive manufacturing[J]. Optics & Laser Technology, 2022, 152: 108146.

[33] ZHOU J, BARRETT R A, LEEN S B. Three-dimensional finite element modelling for additive manufacturing of Ti-6Al-4V components: Effect of scanning strategies on temperature history and residual stress[J]. Journal of Advanced Joining Processes, 2022, 5: 100106.

[34] KHAIRALLAH S A, ANDERSON A T, RUBENCHIK A, et al. Laser powder-bed fusion additive manufacturing: Physics of complex melt flow and formation mechanisms of pores, spatter, and denudation zones[J]. Acta Materialia, 2016, 108: 36-45.

[35] SUNNY S, GLEASON G, BAILEY K, et al. Importance of microstructure modeling for additively manufactured metal post-process simulations[J]. International Journal of Engineering Science, 2021, 166: 103515.

[36] SUNNY S, YU H, MATHEWS R, et al. Improved grain structure prediction in metal additive manufacturing using a dynamic kinetic Monte Carlo framework[J]. Additive Manufacturing, 2021, 37: 101649.

[37] CLOOTS M, UGGOWITZER P J, WEGENER K. Investigations on the microstructure and crack formation of IN738LC samples processed by selective laser melting using Gaussian and doughnut profiles[J]. Materials & Design, 2016, 89: 770-784.

[38] ENGELI R, ETTER T, HÖVEL S, et al. Processability of different IN738LC powder batches by selective laser melting[J]. Journal of Materials Processing Technology, 2016, 229: 484-491.

[39] ZACHARIA T, DAVID S A, VITEK J M, et al. Weld pool development during GTA and laser beam welding of type 304 stainless steel, Part II—Experimental correlation[J]. Welding Journal, 1989, 68(12): 510-519.

[40] FAN H G, TSAI H L, NA S J. Heat transfer and fluid flow in a partially or fully penetrated weld pool in gas tungsten arc welding[J]. International Journal of Heat and Mass Transfer, 2001, 44(2): 417-428.

[41] SHISHKOVSKY I, SHERBAKOF V. Influence of laser cycling on electro-structural features of nickel-titanium SMA fabricated by LPBF process[J]. Applied Surface Science, 2020, 508: 145278.

[42] TANG W, YANG X, TIAN C, et al. Interfacial grain structure, texture and tensile behavior of multilayer deformation-based additively manufactured Al 6061 alloy[J]. Materials Characterization, 2023, 196: 112646.

Acknowledgements This work was supported by the Natural Science Foundation of Shandong Province (No. ZR2021QE230), the Talent Research Project of Qilu University of Technology (Shandong Academy of Sciences) (No.2023RCKY118), and the National Natural Science Foundation of China (Nos.52275438, 52205480).

Author Dr. **LI Binxun** received the M.S. degree in Mechanical Engineering from Liaoning University of Science and Technology, Liaoning, China, in 2016 and Ph.D. degree in Mechanical Engineering from Shandong University, Shandong, China, in 2020, respectively. He joined in Qilu University of Technology (Shandong Academy of Science) in January 2021, where he is a lecture of Faculty of Mechanical Engineering. His research is focused on hybrid additive/subtractive manufacturing, high efficiency machining and finite element modeling as well as relevant fields.

Author contributions Dr. **LI Binxun** designed the study, conducted the analysis, interpreted the results and wrote the

manuscript. Dr. **SUN Yujing** contributed to the discussion and background of the study. Prof. **DU Jin** contributed to the data analysis and funding acquisition. Dr. **XIA Yan** contributed to the finite element modeling. Prof. **SU Guosheng** contributed to the draft and language modification. Mr. **ZHANG Qing** contributed to the subroutine written. All authors commented on the manuscript draft and approved the submission.

Competing interests The authors declare no competing interests.

(Production Editor: WANG Jing)

选区激光熔化镍基合金IN625数值仿真热源模型比较研究

李斌训[1,2], 孙玉晶[1,2], 杜 劲[1,2], 夏 岩[1,2], 苏国胜[1,2], 张 庆[3]

(1.齐鲁工业大学(山东省科学院)机械工程学院,济南 250353,中国; 2.山东省机械设计研究院,济南 250031,中国; 3.山东大学工程训练中心,济南 250002,中国)

摘要:热源模型的选取对数值模拟增材制造过程中准确预测温度场分布和熔池形貌至关重要。本文选取面热源模型、体热源模型和双椭圆热源模型进行对比分析。3种热源模型被汇编成用户自定义子程序嵌入Abaqus/Standard仿真软件中用于镍基高温合金IN625选区激光熔化过程中最高温度和熔池形貌的预测。仿真与实验结果对比表明,双椭圆模型可以较好地预测熔池几何形貌,而体热源模型在预测最高温度值时准确度更好。相比之下,面热源模型在预测最高温度和熔池形貌时准确度最差。研究结果表明,在开展深入研究之前,热源模型的校准修正是提高效率和模拟准确性的前提。

关键词:热源模型;数值仿真;IN625;温度;熔池形貌